

Rising hazard of storm surge is consistent with sea level trend and caused by intensification and widening of tropical cyclone in Japan

Md. Rezuhanul Islam^{a*}, Masaki Satoh^b, Yohei Sawada^a, Le Duc^a

^aInstitute of Engineering Innovation, The University of Tokyo, Tokyo, 113-8656, Japan;

^bAtmosphere and Ocean Research Institute, The University of Tokyo, Kashiwa, 277-0882, Japan

*To whom correspondence should be addressed: Md Rezuhanul Islam

Email: fahim.islam@sogo.t.u-tokyo.ac.jp

Author Contributions: M.R.I. designed research; M.R.I. performed research; M.R.I. analyzed data; M.R.I. wrote the paper; M.S., Y.S., and L.D. supervised the study; and M.S., Y.S., and L.D. edited the paper.

Competing Interest Statement: The authors declare no competing interest.

Keywords: storm surge, sea level rise, tropical cyclone, trend analysis, Japan

Hereby we declare that this paper is a non-peer reviewed preprint submitted to EarthArXiv

Abstract

Variability in storminess, storm surge, and mean sea level (MSL) can substantially alter coastal hazards associated with extreme sea levels (ESL). However, detection and attribution of past changes in tropical cyclone (TC) and related storm surge activity are hampered by inhomogeneous TC records due to changes in observational capabilities. Here we investigate spatiotemporal changes in storm surge levels in Japan from 1980–2019, a period when observational platforms including tide gauges and storm records are highly consistent. The analyses illustrate statistical evidence of increasing surge annual maxima in several places including the bay area of Tokyo since 1980 and this rate of change is comparable to those observed for MSL rise over the same period. These findings contrast the current hypothesis on the flood adaptation plan in which future surge extremes will remain the same. We demonstrate that the change in surge annual maxima reflects the combined effect of a consistent northeastward shifting of TC landfall location, intensifying and widening of TC. The substantial influence of these TC meteorological variables on surge levels coupled with MSL rise over long periods suggests that current coastal planning practices including critical heights for flood defenses, might be inadequate in the future.

Significance Statement

Studies have shown that the ratio of intense TC is expected to increase in the future from present-day values. Nevertheless, current coastal planning practices assume that the statistics of future surge levels will remain the same as those under the current climate. Here, we illustrate that increases in surge annual maxima and MSL rise both contributed to the overall change in ESL in Japan since 1980. Surge level change translates into a combined effect of shifting TC landfall location, increasing intensity and size of TC. The coupled effect of changing TC meteorological variables and MSL rise revealed that the current hypothesis on the flood adaptation plan would turn out to be invalid and cause coastal adaptation plans to be ineffective.

Introduction

Storm surge, a rise in sea level due to tropical cyclone (TC), is a major driver of coastal flooding and has been responsible for as many as 2.6 million deaths worldwide during past 200 years (1). Coastal development results in dense population in low-lying cities roughly five times (241 people/km²) than the global mean (47 people/km²); (2) where storm surge can lead to devastating societal impacts. On average, 0.8–1.1 million people is exposed to coastal flood each year globally (3). Several simulation studies including the Special Report by the Inter-governmental Panel on Climate Change claimed the increase in extreme sea levels (ESL) by 2100 due to storm surge and mean sea level (MSL) rise with high confidence (4–6). Vitousek et al. found that even small changes in ESL (e.g., +10 cm) could substantially induce the change in flooding frequency in many coastal regions between 2030 and 2050 (7). Without adaptation and mitigation measures, flooding can cause adverse effects close to 10% of the global gross domestic product by the end of this century (3). However, the effective implementation of adaptation and mitigation strategies largely depends on a rigorous understanding of the long-term ESL change. ESL is primarily a function of storm surge and MSL change, and other factors include tides and waves. While the ESL change due to mean sea-level rise in recent decades has received greater attention (8–13), the contribution from changes to surge magnitudes remains a grey area that needs to be clarified (14).

The analysis of long-term changes in TC-induced storm surge is missing in many regions due to the unavailability of mid to long-term systematic tide gauge observations. Nonetheless, a few recent observational studies have concluded that storm surge levels are increasing in some regions over time, though the trends are mainly influenced by MSL rise (e.g., 9–11). They interpreted their results as storm surge trends are masked by MSL change. Consequently, previous works on future coastal flood risk assessment, which affect the fundamental of adaptation plans, evaluated the future ESL

by adding the projected MSL change onto the present climate's storm surge level statistics (7, 12, 13). If this assumption of unchanged future storm surge levels turns out to be invalid (either globally or regionally), adaptation plans will be ineffective (15). Due to climate change, the characteristics of TCs are likely to change. Specifically, the proportion of intense tropical cyclones is expected to increase in the future from present-day values, despite the decrease of the total number of TCs. These variations can change storm surge activity and thus ESL (4, 16, 17). Therefore, understanding the compound impacts of changing TC characteristics, storm surge levels, and MSL in altering the likelihood of extreme events (on a global and regional scale) is a pressing matter before making the basis of the coastal adaptation plan final.

Earlier, the contribution from changes in TCs and MSL to storm surge climatology has been studied separately for different time periods and thus the compound association among them is unclear. For instance, Calafat et al. found that extreme storm surges in Europe have increased between 1960 and 2018, which is comparable to the rate of the observed MSL rise. Although their quantified surge trend reflects the contribution from both internal climate variability and anthropogenic forcings (15), its' association with the prevailing TC's meteorological conditions (e.g., intensity, size) has not been discussed. Cole et al., Oey and Chou, and Feng et al. separately showed that TC landfall location, intensity, and translation speed have changed over time and thus modulated surge extremes in their study regions (18–20). The variability in TC size also has the potential to change surge levels (21–23), however, it is not being studied thoroughly from a historical perspective—probably because the operational service for TC size monitoring had just begun at the end of the twentieth century. While these previous observational studies have used one to one relationship (e.g., TC track vs. surge; intensity vs. surge) to explain the contributions from changes in storminess to observed surge levels, their joint influence (e.g., change in storm surge as a function of change in TC intensity and size) is still unknown. The aforementioned deficiencies pose an enormous challenge in understating how storm surge levels modulate ESL under the future climate condition.

Here we provide statistically significant observational evidence that storm surge levels in Japan have increased since 1980 and this rate of change is comparable to those observed for MSL rise. We reveal that a consistent northeastward shift in TC landfall location together with an increased frequency of strong and large sized TCs has attributed to surge level change. We utilize homogeneous records of MSL, TC storm surge, best track, and meteorological data, which the Japan Meteorological Agency (JMA; see data and methods) maintains. This study suggests that current coastal planning practices may need to be reconsidered, which assume an unchanged pattern of surge levels.

Observational evidence of storm surge change

The change rates of surge annual maxima averaged over eastern (R1), western (R2), and southern (R3) Japan are shown in Fig. 1a (left bars). We recall here that only regions with at least 30 years of data have been used and thus excluded northern Japan (R4). An overall increase in the surge magnitude of $+12.1 \text{ mm year}^{-1}$ is evident for 1980–2019. In each region, this change rate varies since storm surge hazards are not spatially homogeneous. While R1 exhibits a maximum change rate of $+16.3 \text{ mm year}^{-1}$ followed by $+10.9 \text{ mm year}^{-1}$ in R2, there is no significant change in R3. A more detailed outlook is plotted for the coastal observation stations in Fig. 1b. It depicts the substantial difference in storm surge climatology between eastern and southern Japan. A significant increasing tendency ($\sim +10 \text{ mm year}^{-1}$) is noticeable around major coastal cities include Tokyo (in R1), Nagoya (in R1), and Osaka (in R2). We further analyze the distribution of storm surge events in Japan between two sub-periods: 1980–1999 (P1) and 2000–2019 (P2) (Fig. 1c). It reveals a clear shift towards greater annual maxima from P1 to P2 as the occurrence frequency is significantly large in each bin (red box). For example, the occurrence frequency of surge annual maxima greater than 100 cm is doubled in P2 than in P1.

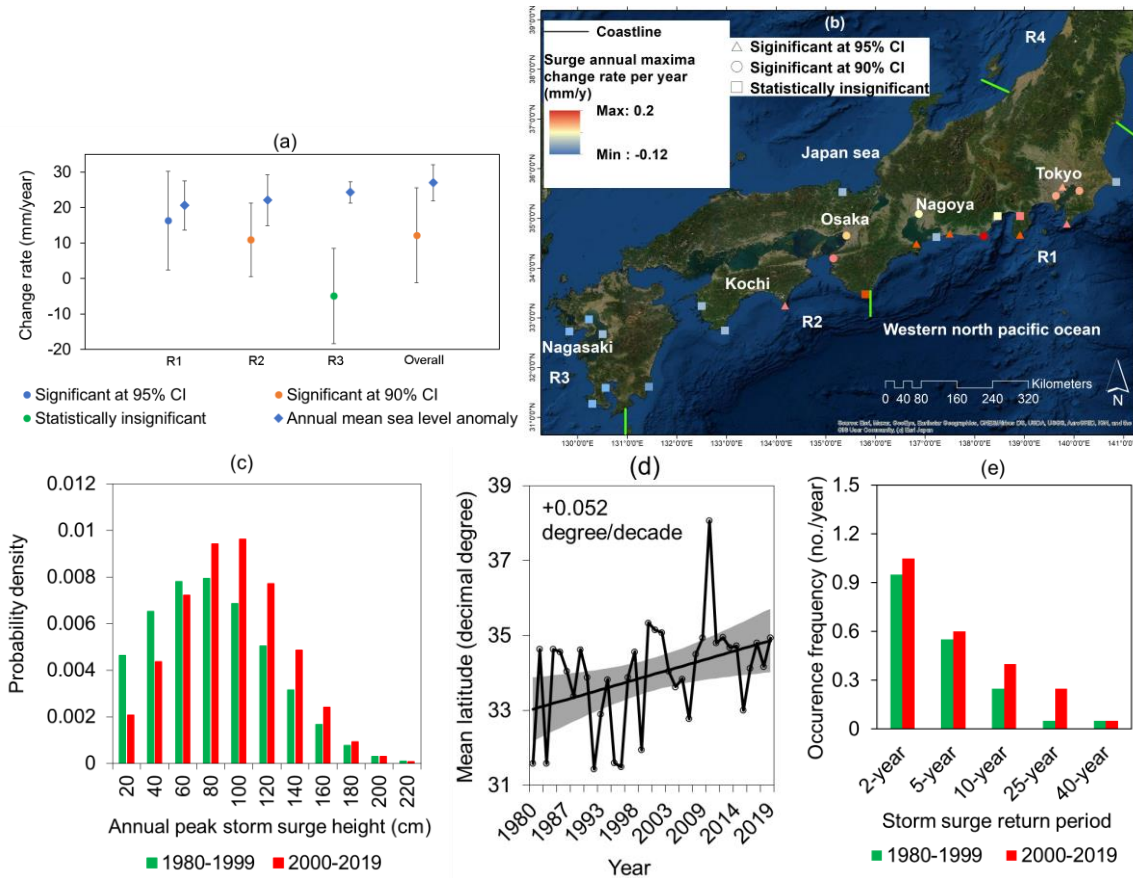


Figure 1. (a) Linear change in surge annual maxima (left bars) and mean sea level (right bars) averaged over the regions R1, R2, and R3 (indicated by the green lines in panel (b)) in Japan during 1980–2019. Whiskers show two-sided confidence intervals (surge annual maxima–R1: 95% CI; R2, R3, and overall: 90% CI; annual MSL anomaly–R1, R2, R3, and overall: 95% CI); (b) Spatial distribution of linear change in surge annual maxima along the Japan coast during the period of 1980–2019; (c) Change in the distribution of surge annual maxima between P1 (1980–1999) and P2 (2000–2019) in Japan; (d) Time series of annual mean latitude of peak storm surge recorded along the Japan coast during 1980–2019. Gray shading indicates the two-sided 95% confidence bounds around the linear regression line. The latitudinal difference averaged over 1980–1999 and 2000–2019 is statistically significant at the 95% CI; (e) Changes in the annual occurrence frequency of storm surge return period in P2 (2000–2019) relative to P1 (1980–1999).

Next, we compare surge change rates (Fig. 1a; left bars) with the average MSL anomaly during 1980–2019 (Fig. 1a; right bars). While the rate of surge height change ($+16.3 \text{ mm year}^{-1}$) is similar to the rate of MSL rise ($+20.6 \text{ mm year}^{-1}$) in R1, the ratio of surge to MSL change rate is 0.5 in R2. In R1 and R2, both surge and MSL change rates are positive implying that their compound effect significantly contributes to increasing ESL. Notably, the MSL rise in R3 ($+24.3 \text{ mm year}^{-1}$) is larger than in the other regions, whereas no compound effect is noticeable as of R1 and R2. Several previous works have shown that MSL is rising along the Japanese coast (24–26), nevertheless, we report the compound effect of storm surge and MSL change for the first time.

When the annual mean latitude for the peak surge locations is calculated in Japan over 1980–2019, there is a clear and statistically significant northeastward change of $+0.052$ degree per decade (Fig. 1d). The northeastward shift of peak surge leads to an increased surge levels in Tokyo (in R1),

Nagoya (in R1), and Osaka (in R2) which are all located above the 34.5° latitude belt. For example, the recorded number of surge annual maxima between the 34.5°–35.5° latitude belt is 1.7 times higher during P2 than during P1.

Following the assessment of changes in surge annual maxima and peak surge location, we also measure changes in the occurrence of different return period surge events (Fig. 1e). It is particularly useful as it helps communicate whether environmental extremes are occurring more or less frequently relative to any chosen point in the past. First, we estimated the magnitude and annual occurrence frequency of a 2-, 5-, 10-, 25-, and 40-year storm surge event for 1980–1999 (see Fig. S2 in SI appendix). Finally, we compare the annual occurrence frequency of similar return level events in P2 (2000–2019) with P1 (1980–1999). Variations in different return periods' surge events mirror the changes in surge magnitude. A gradual increased frequency of small to medium-sized surge events has been observed in a recent 20-year period. For example, the ratio of the 25-year return period surge occurrence frequency in P2 to P1 is five. In Japan, the current storm surge warning criteria is based on the designed tidal level which is equivalent to a return period event (27). Therefore, our findings highlight the importance of regularly updating storm surge warning criteria under changing the return period of observed surge events.

Attribution of changing storm surge level

Here we discuss changes in TC meteorological conditions including track, intensity, size, and translation speed, which can significantly modulate storm surge climatology (21, 22, 28–30). Besides the northeastward shift of peak surge location, there is evidence that TCs occurrence probability along the Pacific coast of the eastern (R1) and western (R2) Japan has increased substantially during P2 than in P1 (Fig. 2a). It corroborates the findings of Kubota et al. (31), who detected a significant northeastward shift of TC landfall location in Japan during 1977–2019. In contrast, TC occurrence frequency has remained almost stationary in R3. One remarkable feature is that the occurrence frequency of landfalling TC in R1 (nationwide) during P1 and P2 are 0.65 (1.85) and 1.15 (2.35) per year, respectively and the difference is statistically significant at the 90% confidence level. Such differences in the TC landfall location and frequency appear to contribute to greater storm surge tendency in P2 than in P1.

Next, we analyzed the differences in TC landfall intensity (V_{max}) along with their six-hourly best track positions between P1 and P2. Overall, the frequency of strong TCs during landfall time frame has increased in last 40 years. For example, landfall TC activity with $66\text{-kt} \leq V_{max} \leq 80\text{-kt}$ (~equivalent to Category 1 Hurricane in Saffir-Simpson Hurricane Wind Scale) has increased significantly in R1 and R2 from P1 to P2 (Fig. 2b). In other words, the occurrence frequency of landfall TC intensity with $66\text{-kt} \leq V_{max} \leq 80\text{-kt}$ has increased by 1.9 times. Similar increasing tendencies are also evident for other wind intensity categories (see Fig. S3 in SI appendix). These findings are consistent with Yamaguchi and Maeda (32), who showed that the frequency of strong TCs with central pressure of less than 980 hPa that approached major Japanese cities (e.g., Tokyo, Nagoya, Osaka) significantly increased during 1980–2019. It is also noticeable that TCs which made landfall in R3 have not changed their landfall intensity (Fig. 2b). In addition to best track intensities, we examined recorded local maximum wind speed for each TC selected in this study (see Fig. S4 in SI appendix). It also depicts that TCs in P2 had caused stronger local winds (e.g., $> 50\text{-kt}$) in R1 particularly during P1. The change in TC intensity and local wind may be attributed to larger storm surge levels observed across R1 and R2.

Fig. 2c shows that the R2 region has been frequently exposed to large TCs ($270\text{ NM} \leq R_{30} \leq 430\text{ NM}$), followed by R1 during landfall time in a recent 20-year period. Here, we adopted JMA's definition to describe the size of a TC (Large TC = $270\text{ NM} \leq R_{30} \leq 430\text{ NM}$; very large = $R_{30} > 430\text{ NM}$; (33)) and provided the density map utilizing six-hourly best track positions along with TC size information. Overall, the frequency of large TC has increased more than fourfold from 1980 to 2019.

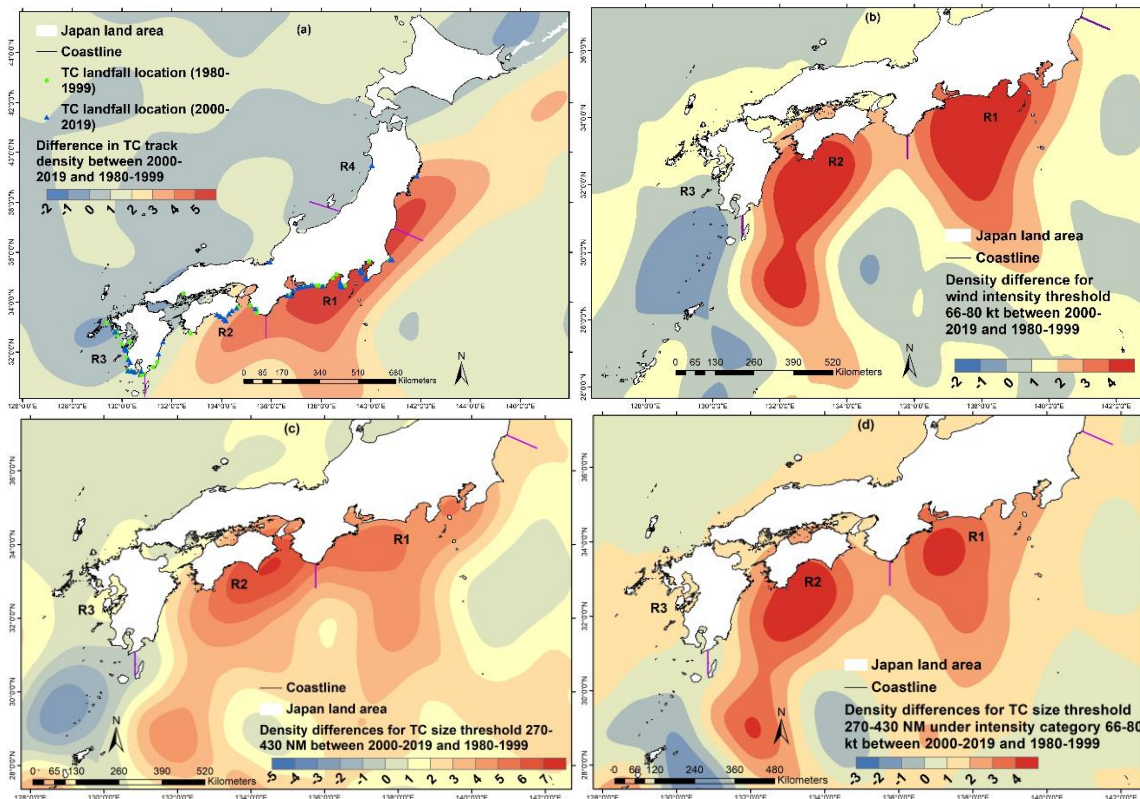


Figure 2. Density differences for landfalling (a) tropical cyclone track; (b) tropical cyclone wind intensity: $66\text{-kt} \leq V_{max} \leq 80\text{-kt}$; (c) Tropical cyclone 30-kt wind radius: $270\text{ NM} \leq R_{30} \leq 430\text{ NM}$; (d) tropical cyclone size: $270\text{ NM} \leq R_{30} \leq 430\text{ NM}$ under wind intensity category 66-80-kt, between P2 (2000–2019; $n = 47$) and P1 (1980–1999; $n = 37$). Six-hourly JMA best track positions along with TC wind intensity (V_{max}) and size (R_{30}) information are utilized to provide density maps.

TC-induced surge dependence over TC size is primarily due to sideways radiation and the dipole nature of the wind stress field. These both become less inhibitive for larger systems and, thus, result in greater surge levels (34). However, it needs to be noted that a smaller but intense TC could also elevate surge levels as the pressure gradient tends to be steep, resulting in stronger winds near the eye of a TC (35). Along with analyzing TC track, intensity, and size, we also investigate the variability of TC translation speed. No apparent changes in frequency were observed during 1980–2019 (e.g., landfall TCs have neither become faster nor slower: see Fig. S5 in SI appendix).

Although Figs. 2(a-c) demonstrate the statistical evidence of the changes in TC meteorological components individually that are responsible for modulating surge hazards in Japan, the amplitude of surge greatly depends on the combined effect of track, intensity, and size. Figure 2d illustrates the changes in the joint occurrence of strong ($66\text{-kt} \leq V_{max} \leq 80\text{-kt}$) and large ($270\text{ NM} \leq R_{30} \leq 430\text{ NM}$) TCs over the past 40 years in Japan. Observational changes in surge annual maxima in R1 and R2, in general, reflect the combined effect of shifting TC landfall location, increasing intensity and size of TC. More explicitly, the integration of storm size and wind strength over the footprint of the TC provides a bulk amount of energy/momentum transferred from the storm to the water column and, thus, the functional dependence of the surge level on the velocity and storm radius. The environmental conditions include the sea surface temperature, vertical wind shear, and relative humidity at 500 hPa, atmospheric circulation conditions, and anthropogenic climate forcings may be responsible for creating favorable conditions for such kind of strong and large TC development

in P2 than in P1 (32, 36); however, a detailed analysis of these processes is beyond the scope of this study.

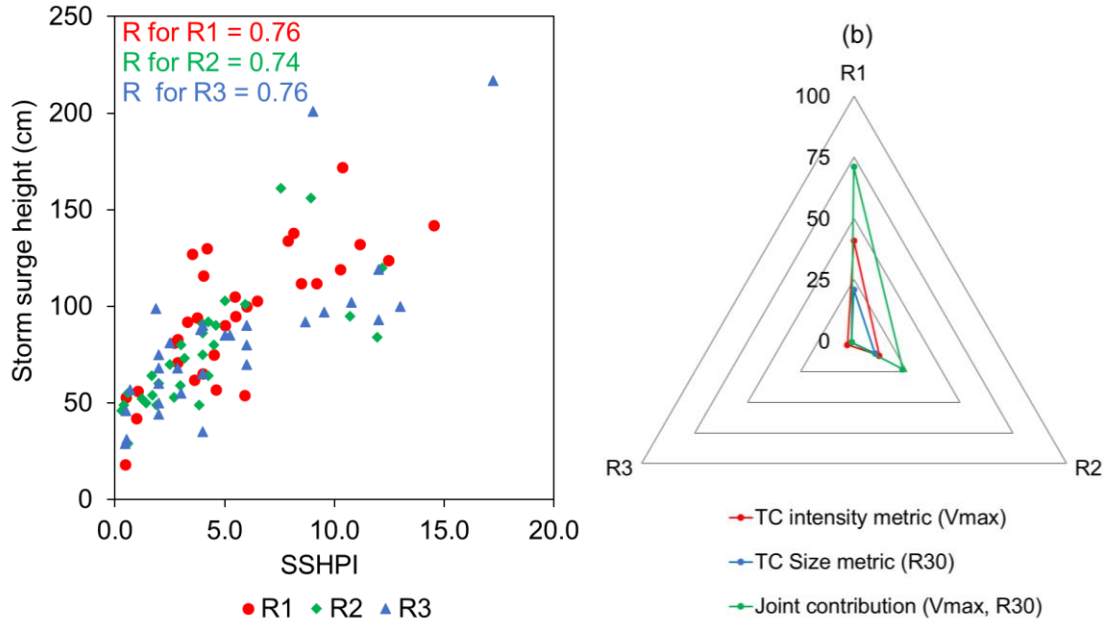


Figure 3. (a) Comparison of the storm surge hazard potential index with surge annual maxima for eastern (R1), western (R2), and southern (R3) Japan during 1980–2019. Stated Pearson correlation co-efficient (R) follows a similar color code respective to each region; **(b)** Possible attribution of tropical cyclone meteorological variables: TC wind intensity (V_{max} ; red), TC size (R_{30} ; blue), joint (green)—TC wind intensity (V_{max}) and size (R_{30}), in changing storm surge levels observed during 1980–2019 in Japan. The contribution (%) is calculated assuming that either one (V_{max} or R_{30}) or a set (V_{max} and R_{30}) of the meteorological components included in SSHPI changed between P2 (2000–2019) and P1 (1980–1999) while maintaining the other variables value at their averages from P1.

The association between change in surge annual maxima and TC meteorological condition has been discussed above from an overall perspective. Quantifying individual and joint contributions of TC meteorological variables is also important to understand how the future might alter surge maxima under human-induced climate change. Therefore, we applied the storm surge hazard potential index (SSHPI) to demonstrate it statistically. We note that the SSHPI is positive proportional to the peak surge height and explains ~57% of the observed variance (Fig. 3a). These statistics are comparable to storm surge estimation obtained from full physical numerical surge models (e.g., 36, 37) which comprehensively account for coastal surge dynamics. Thus, SSHPI is a reasonably good proxy for TC-induced peak surge threat and could be utilized to quantify the contributions of TC meteorological components to hazardous surge height. To estimate the contributions of observed TC meteorological variables over the changes in surge annual maxima, we separately changed two SSHPI components (V_{max} or R_{30}) or a set of components (V_{max} and R_{30}) to their P2 (2000–2019) average values and kept the other components at their P1 (1980–1999) averages. Finally, we enumerated each change that affected total change by comparing P2 and P1 index values (see Table S1 SI appendix). In R1, the changes in TC intensity and size contributed 41% and 21%, respectively and their joint contribution may be responsible for as much as 71% of the surge variance (Fig. 3b). This joint influence statistic gets smaller in R2 (23%) and it has no significant role in R3. Nevertheless, Fig. 3b, in general, mimics TC meteorological conditions

illustrated in Fig. 2. In R1 and R2, there are several places (e.g., Tokyo Bay, Ise Bay (Nagoya), Osaka Bay) where mean coastal bathymetry profiles are less than 10 m (39). Thus, it is reasonable to believe that the increased frequency of strong and large-sized TCs has impacted these shallow coastal areas and attributed them to elevate surge levels.

Conclusion

Here we have addressed notable positive changes in surge annual maxima in eastern and western Japan during 1980–2019. It is primarily due to the northeastward shifting of TC landfall location, intensifying and widening of TC over the recent 20 years (2000–2019). Contrary to what previous studies suggest, changes in surge levels were comparable to those observed for MSL rise, leading to the overall change in ESLs over the last 40 years. This conclusion complements that the Japanese coast will likely experience increasing numbers of extreme storm surge events in the future if the current tendency of TC intensification and widening continues.

Materials and Methods

Tropical cyclone selection

In this study, we utilized JMA best track data archives (40) from 1980 to 2019, including data pertaining to TCs that originated in the western North Pacific and made landfall in the main islands of Japan. The best track data acquired during the pre-satellite era (i.e., before 1980) contain heterogeneities and large uncertainties in the data quality (41, 42) and were therefore ignored. Although the time period processed was relatively short, the period from 1980–2019 was the longest period covered by the JMA with uniform data quality. We followed JMA's definition for identifying a landfall TC and it is when the center of a TC reaches the coastline of the mainland (Honshu, Hokkaido, Kyushu, Shikoku) in Japan (33). We detected the approximate landfall point at which a TC track intersects a coastline using vector data provided by the Geospatial Information Authority of Japan (43). Data collection was limited to TCs with a maximum sustained wind speed (V_{max}) greater than 17 m s⁻¹ (33 kt) during the landfall time frame. Adopting a wind intensity threshold is necessary as TCs are not always powerful (i.e., tropical depressions) and may not produce noticeable storm surges; thus, it would be more meaningful to focus on tropical storms (34 kt $\leq V_{max} \leq$ 63 kt) or stronger TCs (i.e., categories 1, 2 in the Saffir–Simpson Hurricane Wind Scale) for managing disaster risk. Based on the aforementioned criteria, 84 TCs were selected for analysis which also can be regarded as the most economically damaging TCs in Japan.

Tide gauge data

Here, TC-induced storm surge is defined as a tide gauge record component that remains after deducting the MSL and astronomical tide. We considered JMA (44) and Japan Coast Guard (45) operated tidal stations to retrieve peak storm surge information for each TC. It needs to be noted that JMA and Japan Coast Guard publish their tidal observations only after controlling the quality of the initial records and thus, the datasets are free from any abrupt changes such as artificial jumps or shifts. The observed tidal records are hourly, and therefore, the peak surge records used in this study are not necessarily exact peak values. Among many operational stations, data collection was limited to those that satisfied the following five criteria: (a) fell to the right side of a selected TC track and located within the range of radius of 50-kt wind (R_{50} ; radius of 30-kt wind (R_{30}) was used when R_{50} is not available during TC landfall time frame); (b) located on an open coastline or in a bay (stations on islands were excluded); (c) JMA-predicted astronomical tide data (46) were available; (d) elevations of the observation reference plane and the astronomical tide table reference plane were available; and (e) no data gaps occurred when a TC traversed over the station. Given these criteria, 28 tidal stations were considered for recording surge levels which are further divided into four regions, namely eastern (R1: 13), western (R2: 7), southern (R3: 6), and northern (R4: 2) Japan (the locations of the tide gauges are shown in Fig. S1 in SI appendix). JMA provides timeseries of annual MSL anomaly region-wise (same as R1, R2, R3, and R4) (47) and thus, the division enabled us to remove MSL anomaly from respective tide gauge observations and compare

surge records with MSL. Given the tidal station selection criteria, storm surge information was recorded for more than one station for each TC selected in this study leading to a total number of 279 surge events during 1980–2019. The surge annual maxima were used to create annual time series.

TC meteorological data

We analyzed JMA best track datasets (40) for selected TCs ($n = 84$) that include TC central positions, intensities (V_{max}), sizes (R_{50} and R_{30}), and translation speeds. Reconstructed typhoon data for Japan (31) was used to collect local maximum wind speed recorded at the nearest weather station or lighthouse during the passage of a TC. It needs to be noted that stations used for recording local maximum wind speed are different from tidal stations used for recording surge levels and thus, we defer to Kubota et al. (31) for full details on the selection of weather stations used for recording local wind speed. Although TC meteorological information available from birth to death were analyzed, we particularly compare TC meteorological conditions during landfall time frame with peak surge records. It is because storm surges tend to be amplified during landfall. However, TC characteristics during the landfall time frame are not necessarily the most adverse conditions to cause the largest storm surges on the coasts. For example, storm surges would take the largest value when the TC track is closer to the bay. In this study, we considered TC landfall time rather than the time closest to each tidal station as a representative condition of causing a peak surge because (a) TC characteristics (i.e., intensity, size, translation speed) after landfall differ from those over the ocean, and thus, the TC information over land is considered less reliable (48); (b) although the recent TC best track contains more detailed information about when a TC approaches the land, the JMA best track has historically provided TC information at 6-h intervals, making it difficult to identify the time of closest approach to a tidal station; (c) in the current dataset, surge information was recorded for more than one tidal station for each TC. Thus, a unique characteristic (e.g., landfalling TC intensity) for each storm can provide a simple basis for statistical analysis.

Storm surge hazard potential index

Previous studies (e.g., 48, 49) reported that a measure of storm surge intensity is worth for estimating TC potential impact. Here, we used the storm surge hazard potential index (SSHPI; 38) to statistically quantify the contributions of meteorological factors that modulated surge hazards during 1980–2019 in Japan. The SSHPI incorporates meteorological variables sensitive to storm surge, including TC intensity, size, and translation speed, along with coastal geometry (open coasts and bays) and regional scale bathymetry into a single measure of the expected surge hazard potential along the coast. TC best track data, particularly during landfall, was used to calculate the SSHPI for each storm. Large surge index values manifest what a TC can pose a surge threat at the time of landfall. The bathymetry of the target region was obtained from the Japan Oceanographic Data Center (52). The effectiveness of the SSHPI for predicting peak surge hazard potential was discussed in Islam et al. (51). A brief definition is provided in the SI appendix.

The temporal changes in storm surge height, peak surge location, and MSL were estimated by linear model to the annual time series using ordinary least squares. The return period for a surge event was calculated as the inverse of $1 - F$ (surge height; location, scale, and shape parameter), in which F is the cumulative distribution function of the generalized extreme value distribution. We divided the 40-year dataset into two sub-periods, 1980–1999 and 2000–2019, hereafter, referred to as P1 and P2, respectively. The two-tailed Student's t -test was used to determine whether the means of any two sets of data were significantly different. Statistical significance was based on the two-sided 95% and 90% confidence intervals (CI) and any statistical value outside the 90% CI was regarded as statistically insignificant.

Acknowledgments

This work is supported by JST FOREST program (grant no. JPMJFR205Q) and JST Moonshot R&D project (grant no. JPMJMS2281).

References

1. R. J. Nicholls, “An expert assessment of storm surge ‘hotspots’” (Center for Hazards and Risk Research, Lamont-Doherty Observatory, Columbia University, Flood Hazard Research Centre, University of Middlesex, 2003).
2. B. Neumann, A. T. Vafeidis, J. Zimmermann, R. J. Nicholls, Future coastal population growth and exposure to sea-level rise and coastal flooding - A global assessment. *PLoS ONE* **10** (2015).
3. J. Hinkel, *et al.*, Coastal flood damage and adaptation costs under 21st century sea-level rise. *Proceedings of the National Academy of Sciences* **111**, 3292–3297 (2014).
4. T. Knutson, *et al.*, Tropical cyclones and climate change assessment part II: Projected response to anthropogenic warming. *Bulletin of the American Meteorological Society* **101**, E303–E322 (2020).
5. S. Muis, *et al.*, A High-Resolution Global Dataset of Extreme Sea Levels, Tides, and Storm Surges, Including Future Projections. *Frontiers in Marine Science* **7** (2020).
6. M. Oppenheimer, *et al.*, “Sea Level Rise and Implications for Low-Lying Islands, Coasts and Communities” (2019) (June 21, 2022).
7. S. Vitousek, *et al.*, Doubling of coastal flooding frequency within decades due to sea-level rise. *Sci Rep* **7**, 1399 (2017).
8. P. D. Bromirski, R. E. Flick, D. R. Cayan, “Storminess Variability along the California Coast: 1858-2000” (2003).
9. P. L. Woodworth, D. L. Blackman, Evidence for systematic changes in extreme high waters since the mid-1970s. *Journal of Climate* **17**, 1190–1197 (2004).
10. J. A. Church, J. R. Hunter, K. L. McInnes, N. J. White, Sea-level rise around the Australian coastline and the changing frequency of extreme sea-level events. *Australian Meteorological Magazine* **55**, 253–260 (2006).
11. M. Menéndez, P. L. Woodworth, Changes in extreme high water levels based on a quasi-global tide-gauge data set. *Journal of Geophysical Research* **115**, C10011 (2010).
12. M. Taherkhani, *et al.*, Sea-level rise exponentially increases coastal flood frequency. *Sci Rep* **10**, 6466 (2020).
13. E. Kirezci, *et al.*, Projections of global-scale extreme sea levels and resulting episodic coastal flooding over the 21st Century. *Sci Rep* **10**, 11629 (2020).
14. , “Intergovernmental Panel on Climate Change in Climate Change 2013: The Physical Science Basis. . Contribution of Working Group I to the Fifth Assessment Report of the

- Intergovernmental Panel on Climate Change (eds Stocker, T. F. et al.)” (2013) (June 22, 2022).
15. F. M. Calafat, T. Wahl, M. G. Tadesse, S. N. Sparrow, Trends in Europe storm surge extremes match the rate of sea-level rise. *Nature* **603**, 841–845 (2022).
 16. T. Knutson, *et al.*, Tropical cyclones and climate change assessment. *Bulletin of the American Meteorological Society* **100**, 1987–2007 (2019).
 17. N. Bloemendaal, *et al.*, A globally consistent local-scale assessment of future tropical cyclone risk. *Science Advances* **8**, eabm8438 (2022).
 18. B. A. Colle, K. Rojowsky, F. Buonaito, New York City Storm Surges: Climatology and an Analysis of the Wind and Cyclone Evolution. *Journal of Applied Meteorology and Climatology* **49**, 85–100 (2010).
 19. L.-Y. Oey, S. Chou, Evidence of rising and poleward shift of storm surge in western North Pacific in recent decades. *Journal of Geophysical Research: Oceans* **121**, 5181–5192 (2016).
 20. X. Feng, *et al.*, Typhoon storm surge in the southeast Chinese mainland modulated by ENSO. *Sci Rep* **11**, 10137 (2021).
 21. J. L. Irish, D. T. Resio, J. J. Ratcliff, The influence of storm size on hurricane surge. *Journal of Physical Oceanography* **38**, 2003–2013 (2008).
 22. M. R. Islam, H. Takagi, Typhoon parameter sensitivity of storm surge in the semi-enclosed Tokyo Bay. *Frontiers of Earth Science* **14**, 553–567 (2020).
 23. M. R. Islam, M. Satoh, H. Takagi, Tropical Cyclones Affecting Japan Central Coast and Changing Storm Surge Hazard since 1980. *Journal of the Meteorological Society of Japan. Ser. II* **100**, 493–507 (2022).
 24. T. Senjyu, M. Matsuyama, N. Matsubara, Interannual and Decadal Sea-Level Variations along the Japanese Coast. *Journal of Oceanography* **55**, 619–633 (1999).
 25. T. Yasuda, K. Sakurai, Interdecadal variability of the sea surface height around Japan. *Geophysical Research Letters* **33** (2006).
 26. Y. N. Sasaki, R. Washizu, T. Yasuda, S. Minobe, Sea Level Variability around Japan during the Twentieth Century Simulated by a Regional Ocean Model. *Journal of Climate* **30**, 5585–5595 (2017).
 27. J. Hasegawa, Y. Takagi, Y. Tsuboi, Key techniques for Japan’s Risk-based Warning Services for Heavy-rain Related Disasters (2017) (June 10, 2022).

28. J. L. Rego, C. Li, Nonlinear terms in storm surge predictions: Effect of tide and shelf geometry with case study from Hurricane Rita. *Journal of Geophysical Research: Oceans* **115** (2010).
29. A. Sebastian, *et al.*, Characterizing hurricane storm surge behavior in Galveston Bay using the SWAN+ADCIRC model. *Coastal Engineering* **88**, 171–181 (2014).
30. M. R. Islam, H. Takagi, Statistical significance of tropical cyclone forward speed on storm surge generation: retrospective analysis of best track and tidal data in Japan. *Georisk* (2020) <https://doi.org/10.1080/17499518.2020.1756345>.
31. H. Kubota, *et al.*, Tropical cyclones over the western north Pacific since the mid-nineteenth century. *Climatic Change* **164**, 29 (2021).
32. M. Yamaguchi, S. Maeda, Increase in the number of tropical cyclones approaching Tokyo since 1980. *Journal of the Meteorological Society of Japan* **98**, 775–786 (2020).
33. JMA, Japan Meteorological Agency | Forecast terms Term related to typhoons (2021) (January 29, 2021).
34. P. Nielsen, How storm size matters for surge height. *Coastal Engineering* **56**, 1002–1004 (2009).
35. M. R. Islam, H. Takagi, “On the Importance of Typhoon Size in Storm Surge Forecasting” in *Water, Flood Management and Water Security Under a Changing Climate: Proceedings from the 7th International Conference on Water and Flood Management*, A. Haque, A. I. A. Chowdhury, Eds. (Springer International Publishing, 2020), pp. 153–162.
36. K. S. Liu, J. C. L. Chan, Interdecadal variation of frequencies of tropical cyclones, intense typhoons and their ratio over the western North Pacific. *International Journal of Climatology* **40**, 3954–3970 (2020).
37. K. T. Mandli, C. N. Dawson, Adaptive mesh refinement for storm surge. *Ocean Modelling* **75**, 36–50 (2014).
38. R. Marsooli, N. Lin, Numerical Modeling of Historical Storm Tides and Waves and Their Interactions Along the U.S. East and Gulf Coasts. *Journal of Geophysical Research: Oceans* **123**, 3844–3874 (2018).
39. N. Mori, N. Ariyoshi, T. Shimura, T. Miyashita, J. Ninomiya, Future projection of maximum potential storm surge height at three major bays in Japan using the maximum potential intensity of a tropical cyclone. *Climatic Change* **164**, 25 (2021).
40. JMA, Japan Meteorological Agency | RSMC Tokyo - Typhoon Center | Best Track Data (2020a) (March 13, 2021).
41. K. T. F. Chan, Are global tropical cyclones moving slower in a warming climate? *Environ. Res. Lett.* **14**, 104015 (2019).

42. I.-J. Moon, S.-H. Kim, J. C. L. Chan, Climate change and tropical cyclone trend. *Nature* **570**, E3–E5 (2019).
43. Geospatial Information Authority of Japan, Global Map Japan (June 30, 2022).
44. Japan Meteorological Agency, Tidal observation data (June 30, 2022).
45. Japan Oceanography Data Center, Tide Stations (2021) (January 8, 2021).
46. JMA, Japan Meteorological Agency, Predicted Tide Stations (2020c) (January 8, 2021).
47. Japan Meteorological Agency, Sea level (around Japan) (June 30, 2022).
48. X. Huang, *et al.*, Evaluation and Error Analysis of Official Tropical Cyclone Intensity Forecasts during 2005–2018 for the Western North Pacific. *Journal of the Meteorological Society of Japan. Ser. II* **99**, 139–163 (2021).
49. K. Zhang, B. C. Douglas, S. P. Leatherman, Twentieth-Century Storm Activity along the U.S. East Coast. *Journal of Climate* **13**, 1748–1761 (2000).
50. A. Grinsted, J. C. Moore, S. Jevrejeva, Homogeneous record of Atlantic hurricane surge threat since 1923. *Proceedings of the National Academy of Sciences* **109**, 19601–19605 (2012).
51. M. R. Islam, C.-Y. Lee, K. T. Mandli, H. Takagi, A new tropical cyclone surge index incorporating the effects of coastal geometry, bathymetry and storm information. *Sci Rep* **11**, 16747 (2021).
52. Japan Oceanographic Data Center, 500m Gridded Bathymetry Data (2020) (January 8, 2021).